

Crystal polymorphism in electrospun composite nanofibers of poly(vinylidene fluoride) with nanoclay

Lei Yu, Peggy Cebe*

Department of Physics and Astronomy, Tufts University, STC-208, 4 Colby Street, Medford, MA 02155, USA

ARTICLE INFO

Article history:

Received 14 January 2009

Received in revised form

25 February 2009

Accepted 1 March 2009

Available online 11 March 2009

Keywords:

PVDF

Electrospinning

Nanocomposites

ABSTRACT

We investigated for the first time the morphology and crystal polymorphism of electrospun composite nanofibers of poly(vinylidene fluoride) (PVDF) with two nanoclays: Lucentite™ STN and SWN. Both nanoclays are based on the hectorite structure, but STN has organic modifier in between the layers of hectorite while SWN does not. PVDF/nanoclay was dissolved in *N,N*-dimethylformamide/acetone and electrospun into composite nanofiber mats with fiber diameters ranging from 50–800 nm. Scanning electron microscopy shows that addition of STN and SWN can greatly decrease the number of beads and make the diameter of the nanofibers more uniform due to the increase of electrospinning solution conductivity brought by the nanoclay. Infrared spectroscopy and X-ray diffraction confirm that both STN and SWN can induce more extended PVDF chain conformers, found in beta and gamma phase, while reducing the alpha phase conformers in electrospun PVDF/Nanoclay composite nanofibers. With the attached organic modifier, even a small amount of STN can totally eliminate the non-polar alpha crystal conformers while SWN cannot. The ionic organic modifier makes STN much more effective than SWN in causing crystallization of the polar beta and gamma phases of PVDF. An ion–dipole interaction mechanism, suggested by Ramasundaram, et al. is utilized to explain the crystal polymorphism behavior in electrospun PVDF/nanoclay composite nanofibers.

© 2009 Elsevier Ltd. All rights reserved.

1. Introduction

Polymer nanocomposites have gained extensive attention in the past decade due to the improvement of the physical properties, such as higher moduli, improved thermal properties, and better barrier properties compared with the original polymer matrix. They are also used in various commercial applications, such as vehicle components and beverage containers [1,2]. Electrospinning is an efficient way to produce electrospun nanofibers with diameters on the order of several hundreds of nanometers. Because of their tiny dimension and high porosity, electrospun nanofiber mats shows a diversity of potential applications including biomedical tissue materials, filtration membranes, polymer electrolytes, and drug delivery membranes [3–8].

The polymer we used in our study is poly(vinylidene fluoride) (PVDF), which is a flexible and light weight semicrystalline thermoplastic with application as transducer film in scientific instruments, and for use as paint and in pipes [9,10]. There are 5 distinct crystal phases found in PVDF [11]: the non-polar TGTC' α and

δ phase, the polar TTTT β phase, and TTTGTTG' γ and ϵ phase, in which T and G are the trans and gauche chain conformations found in PVDF crystal. Alpha is the usual phase formed when PVDF is cooled from melts. Beta phase, which is the most intriguing one due to its piezoelectric and pyroelectric properties, can be formed in a variety of ways, such as mechanical stretching [12–14], high electric field poling of alpha phase film [13–17], and the addition of organically modified nanoclay [18–20]. Gamma phase can be obtained by the transformation from alpha phase upon heating, and by slowly melting samples initially containing beta phase [21,22].

The initial report by Priya and Jog [18] demonstrated that addition of organically modified silicates (OMS) into PVDF films resulted in formation of the polar beta phase. Subsequently, our group [20] and Dillon, et al. [19], investigated PVDF/OMS nanocomposite film using X-ray scattering, differential scanning calorimetry (DSC) and Fourier transform infrared spectroscopy (FTIR). Our research [20] showed that beta phase crystals grew preferentially as more Lucentite™ STN nanoclay was added. In cold crystallized nanocomposites, the alpha crystallographic phase of PVDF was completely suppressed, even at extremely low concentrations of Lucentite™ STN nanoclay [20]. A recent report by Ramasundaram et al. [23] also investigated Lucentite™ STN's impact on

* Corresponding author. Tel.: +1 617 627 3365.

E-mail address: peggy.cebe@tufts.edu (P. Cebe).

PVDF melt crystallization process, and an ion–dipole interaction model was presented. The interaction of the clay nanoparticles with the PVDF molecular chain dipole resulted in preferential formation of the beta phase.

Other than the film sample, neat PVDF electrospun (ES) nanofiber mats have been studied recently [24,25], and the result showed that alpha and beta phase generally co-exist in the electrospun fiber. But by adding tetrabutylammonium chloride (TBAC) ions, pure beta PVDF nanofiber could be formed from electrospinning. Yee, et al. [24] explained their results by the effects of the TBAC ions, which could retain water molecules which then formed hydrogen bonds with the fluorine atoms in PVDF monomers, enhancing the formation of beta. Andrew, et al. [25,33] also showed that by adding Ni–Zn ferrite nanoparticles into PVDF, the beta and gamma phases, containing longer trans sequences, were enhanced in the composite electrospun fibers.

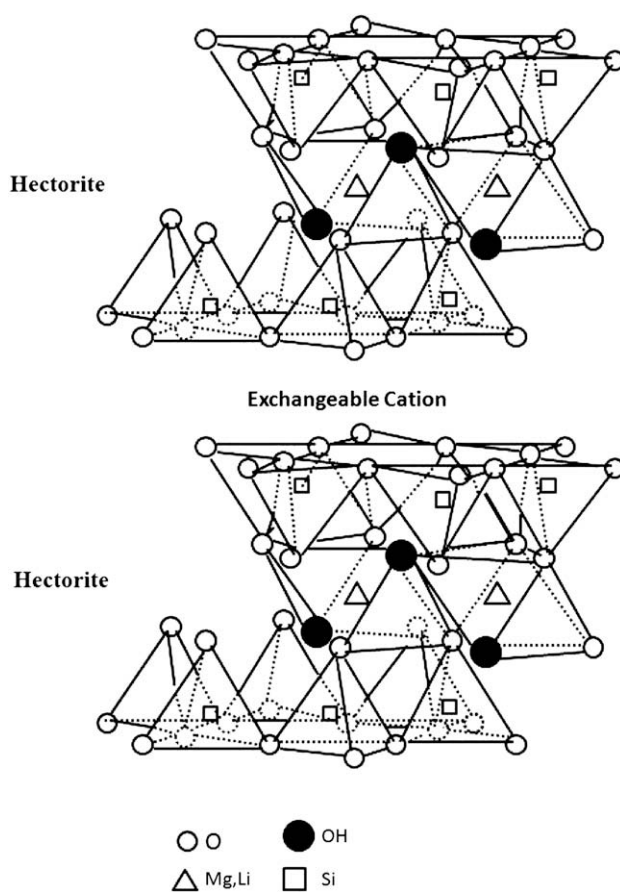
PVDF/Nanoclay composite films and electrospun neat PVDF fibers have been studied previously but as yet there is no research discussing the electrospun composite nanofibers of PVDF with Nanoclay. In our present work, we studied the morphology and polymorphism of electrospun PVDF/Nanoclay composite nanofibers. We used two different nanoclays: Lucentite™ STN and SWN, in which only the former contains an organic modifier. Our results show that both nanoclays can be electrospun with the PVDF matrix forming a composite nanofiber. STN and SWN both have the effect of inducing more beta and gamma phase structure while impeding the growth of alpha phase. But STN is much more effective than SWN because it has ionic organic modifier attached between its silicate layers. We also discuss the mechanism describing how the nanoclay interacts with the polymer chains and induces more polar beta and gamma phase to form, using the model proposed by Ramasundaram, et al. [23].

2. Experimental

2.1. Materials and sample preparation

PVDF used in this study is a Kynar based resin, obtained from Elf Autochem as grade 740, in pellet form. Lucentite™ SWN and STN were the synthetic nanofillers, provided by CBC Chemical Company (Japan) as fine powder. STN is an organically modified layered silicate, which is a mixture of hectorite ($\text{Na}_{0.33}(\text{Mg}_{2.67}\text{Li}_{0.33})(\text{Si}_4\text{O}_{10})(\text{OH})_2$) and tri octyl methyl ammonium ion ($[\text{C}_8\text{H}_{17}]_3(\text{CH}_3)\text{N}^+$). The ionic modifier is located between two layers of hectorite and will not be dissolved into free ion status in the *N,N*-dimethylmethanamide (DMF) solvent we used in our fiber preparation. The content of STN by weight percentage is 68–78% hectorite and 22–32% ionic modifier, according to the manufacturer. The other nanoclay, Lucentite™ SWN, only contains the hectorite without any organic modifier. The structure of the nanoclay is shown in Scheme 1.

A solvent mixture was prepared of dimethylformamide (DMF) and acetone with volume ratio 4:1 DMF/acetone. We prepared five solutions with different PVDF/Nanoclay weight ratios: 0, 0.2, 1, 5 and 10 wt%. At first, a calculated amount of Lucentite™ STN/SWN was dispersed in the DMF/acetone solvent mixture based on the desired PVDF/Nanoclay weight ratio. Then we added PVDF pellets and kept stirring them for 2 days at 40–50 °C until dissolution. The PVDF/solvent weight/volume ratios for all the final solutions were 25% solid but the solutions contained different amounts of nanoclay. For the electrospinning operation, the solutions were then placed into a slightly tilted pipette with a metal needle electrode, connected with the 20 kV voltage, inserted into it. The collector was a grounded plate covered by aluminum foil. Distance between the pipette and the collector plate is around 10 cm. The static electric



Scheme 1. Structure of Lucentite™ nanoclay. The exchangeable cation for STN is $[\text{C}_8\text{H}_{17}]_3(\text{CH}_3)\text{N}^+$; SWN has Na^+ as cation. The scheme is drawn after literature provided courtesy of CBC Chemical Company (Japan), with slight modification.

force between the pipette tip and plate electrospayed the solution, and a composite nanofiber non-woven mat was collected on the aluminum foil.

2.2. Analysis methods

Room temperature wide angle X-ray scattering (WAXS) studies were performed using a Bruker D8 Discover X-ray diffractometer with X-ray wavelength $\lambda = 0.1542$ nm, operated at 40 kV and 20 mA. Data were collected in transmission mode for 5 min. Air background was subtracted, and the 2-D isotropic image was converted to a 1-D scan by integration over a sector. Differential scanning calorimetry (DSC) was performed on a TA Instruments Q100 Modulated DSC at a heating rate of 10 °C/min for all PVDF/nanoclay electrospun fiber. Indium was employed for the temperature and heat flow calibration. The sample weight was 5–10 mg. The degree of crystallinity of PVDF was determined from the endotherm area using 104.6 J/g as the heat of fusion of 100% crystalline PVDF. [26] Fourier transform infrared spectroscopy (FTIR) spectra were collected using a JASCO FTIR System in attenuated total reflectance (ATR) mode. The scanning range is from 4000 to 400 cm^{-1} . A total of 64 scans were collected for signal averaging with resolution of 4 cm^{-1} . Scanning Electron Microscopy (SEM) was used to study the morphology of the electrospun fibers using a Zeiss Ultra 55 SEM system at the Harvard Center for Nanoscale Systems. A thin layer of gold was sputtered on the sample before putting into the SEM vacuum chamber.

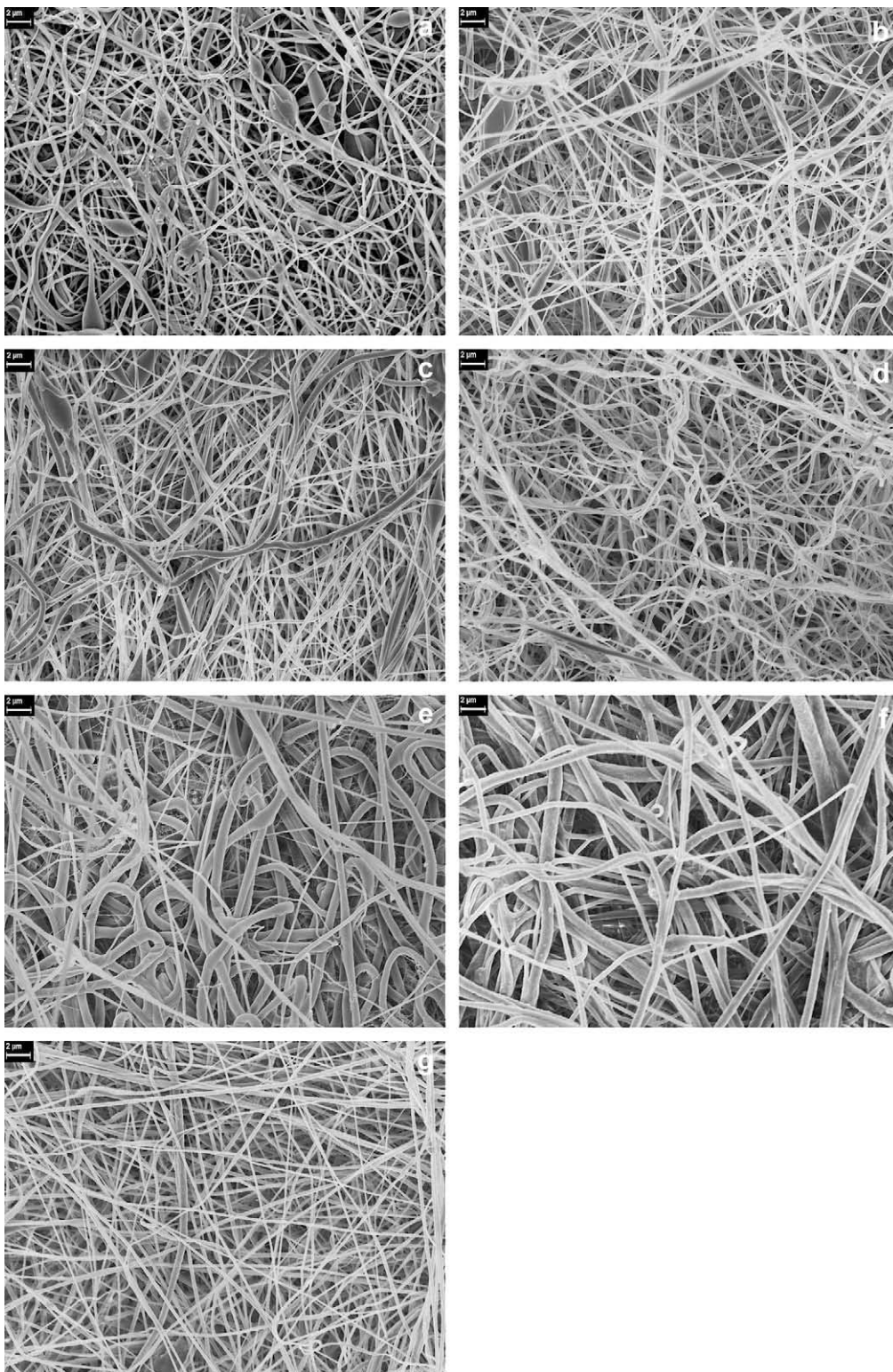


Fig. 1. SEM images of electrospun composite nanofibers of PVDF/Nanoclay with different nanoclay contents: (a) 0.0 wt% (pure PVDF); (b) 0.2 wt% STN; (c) 1.0 wt% STN; (d) 5.0 wt% STN; (e) 10.0 wt% STN; (f) 1.0 wt% SWN; (g) 10.0 wt% SWN. Electrospinning voltage is 20 kV and source-to-collector distance is 10 cm. The scale bar represents 2 microns.

3. Results and discussion

3.1. Electrospun fiber morphology

Fig. 1a–g shows SEM images of pure PVDF (Fig. 1a) and PVDF/Nanoclay composite nanofibers electrospun at voltage of 20 kV

from 25 wt% PVDF/Nanoclay solution containing varying amounts of STN (Fig. 1b–e) or SWN (Fig. 1f,g). The SEM images show that the diameters of the nanofibers in pure PVDF are not uniform and diameter ranges between 50 nm and 700 nm.

Irregularly shaped beads are present in the pure PVDF nanofiber mat with diameter at the bead center varying between

0.8 μm and 3 μm . As the concentration of nanoclay increased the diameters of the nanofibers became more uniform, and the beads became smaller and less numerous. Fig. 2 shows the comparison of fiber diameter distribution between electrospun PVDF and 1% STN or SWN composite nanofiber. The diameters of electrospun PVDF fibers range from around 50–700 nm, but for 1% nanoclay composite nanofiber, the diameters range from 100–350 nm for STN and 300–800 nm for SWN. The standard deviation of the diameter for the electrospun PVDF nanofiber is 178 nm while for the composite nanofiber is 51 nm for STN and 136 nm for SWN. Addition of STN makes the nanofibers thinner while SWN shows the opposite effect. This can be explained by the larger viscosity of electrospinning solution containing SWN compared to STN, since higher viscosity favors thicker fibers. Both STN and SWN make the diameter of the nanofiber more uniform, which is because of the increase of solution conductivity with the addition of nanoclay. Addition of nanoclay to PVDF has the effect to greatly reduce the occurrence of beads. Increase of the conductivity of the electrospinning solution is known to decrease the formation of beads. [27] Therefore, the decrease of bead formation with the nanoclay addition is due to the electrical charges on both hectorite and the organic modifier, both of which will increase solution conductivity.

3.2. Crystal polymorphism in ES fibers

Fig. 3a,b shows WAXS patterns for electrospun PVDF composite nanofibers with STN and SWN, respectively. Homopolymer PVDF electrospun nanofiber shows X-ray diffraction peaks at 18.6° , and 20.6° , and 27.1° (for $\lambda = 0.154 \text{ nm}$) which are indexed to, respectively, $\alpha(020)$, $\beta(200/110)$, and $\alpha(111)/\alpha(021)$ reflections for PVDF crystalline conformation [28,29]. As more STN or SWN is added, all the α peaks diminish and the β peak increases. In 1%, 5%, and 10% STN nanocomposite samples, only the peak for beta phase and the amorphous halo can be seen. SWN nanocomposite samples retain some fraction of alpha phase, even at 10% SWN addition. Regarding the polar gamma phase, gamma has WAXS reflections that overlap reflections of the alpha phase crystal; $\alpha(100)$ is the only WAXS peak that has no overlap with gamma phase. Therefore, based on our X-ray scattering data alone, we cannot separately identify gamma phase from alpha phase. For this reason, we use FTIR to identify existence of the gamma phase, which will be discussed later.

To determine the crystallinity index from the WAXS patterns, we fitted the crystalline peaks and determined the area ratio of the crystal peaks to the total area of coherent scattering. The Lorentz-corrected scattered intensity, Iq^2 vs. q was fitted with a sum of Gaussians and a quadratic baseline:

$$I(q)q^2 = \sum \left\{ A_i \exp\left(\frac{(q - q_{0i})^2}{2\sigma_i^2}\right) \right\} + Bq + Cq^2 \quad (1)$$

where A_i is the amplitude, q_{0i} is the mean q -vector, σ_i is the standard deviation, and B and C are the q and q^2 coefficients of the quadratic, respectively. An example of the fitting is shown in Fig. 3c for the electrospun unfilled PVDF nanofibers. From the fit of the X-ray curves, we determined the mass fraction crystallinity index (crystal peak area ratio to total area) and the mass ratio of alpha to beta phase crystals (alpha peak area to beta peak area) for PVDF and composite nanofibers as listed in Table 1.

Data in Table 1 show the addition of SWN and STN both tend to decrease the crystallinity of the nanofibers compared to its value in electrospun PVDF homopolymer. The nanoclay can reduce the chain mobility causing constraints [20] and thus would impede the growth of crystals. This is a possible cause of why the overall crystallinity decreases with addition of SWN and STN. During electrospinning, the clay platelets of SWN and STN bond with PVDF

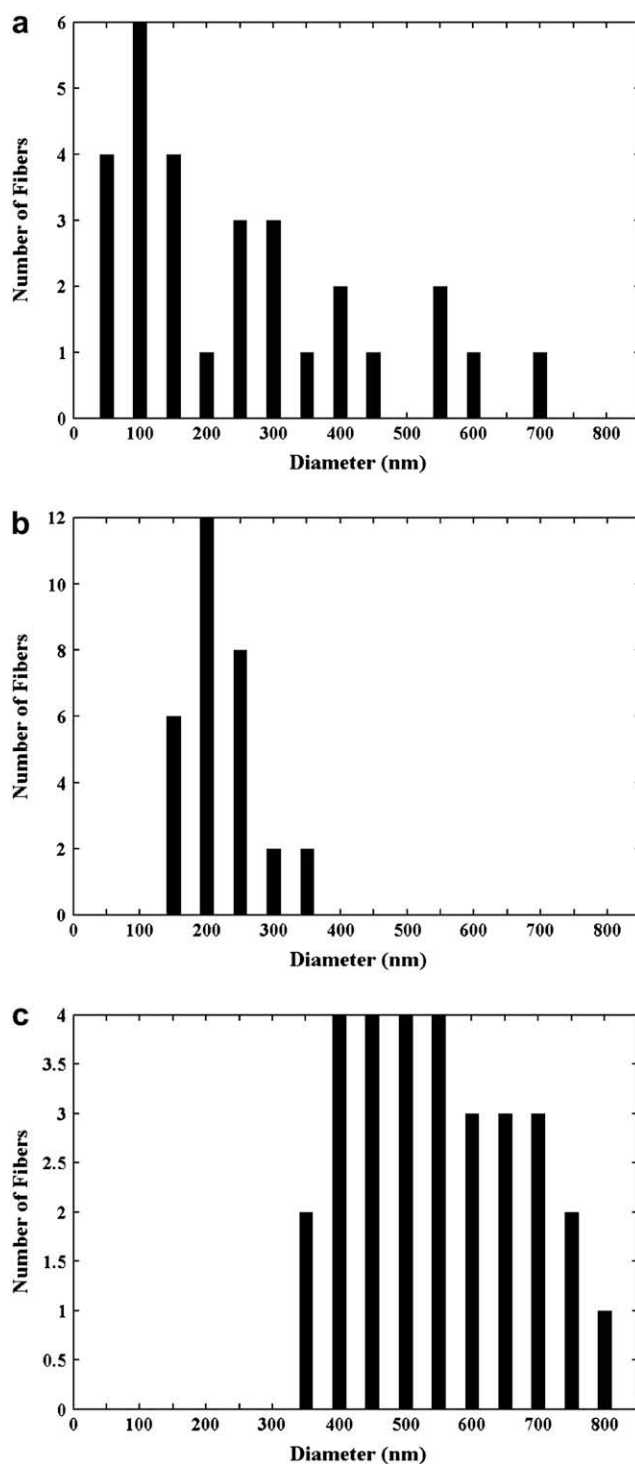


Fig. 2. Diameter distribution for electrospun composite nanofibers: (a) PVDF; (b) PVDF/STN 1.0%; (c) PVDF/SWN 1.0%.

chains, causing greater orientation (discussed later in Section 3.3) of chains along the fiber axis, impeding chain folding. This has the impact of reducing the overall crystallinity in ES fibers containing STN or SWN clay.

Both SWN and STN increase the relative amount of the beta phase crystals while decreasing the alpha phase. But adding 1% or more of STN can completely prevent alpha phase crystal from forming, and only beta phase is observed in PVDF/STN 1%, 5%, and 10% composite nanofibers. Composite nanofibers made with 1% and

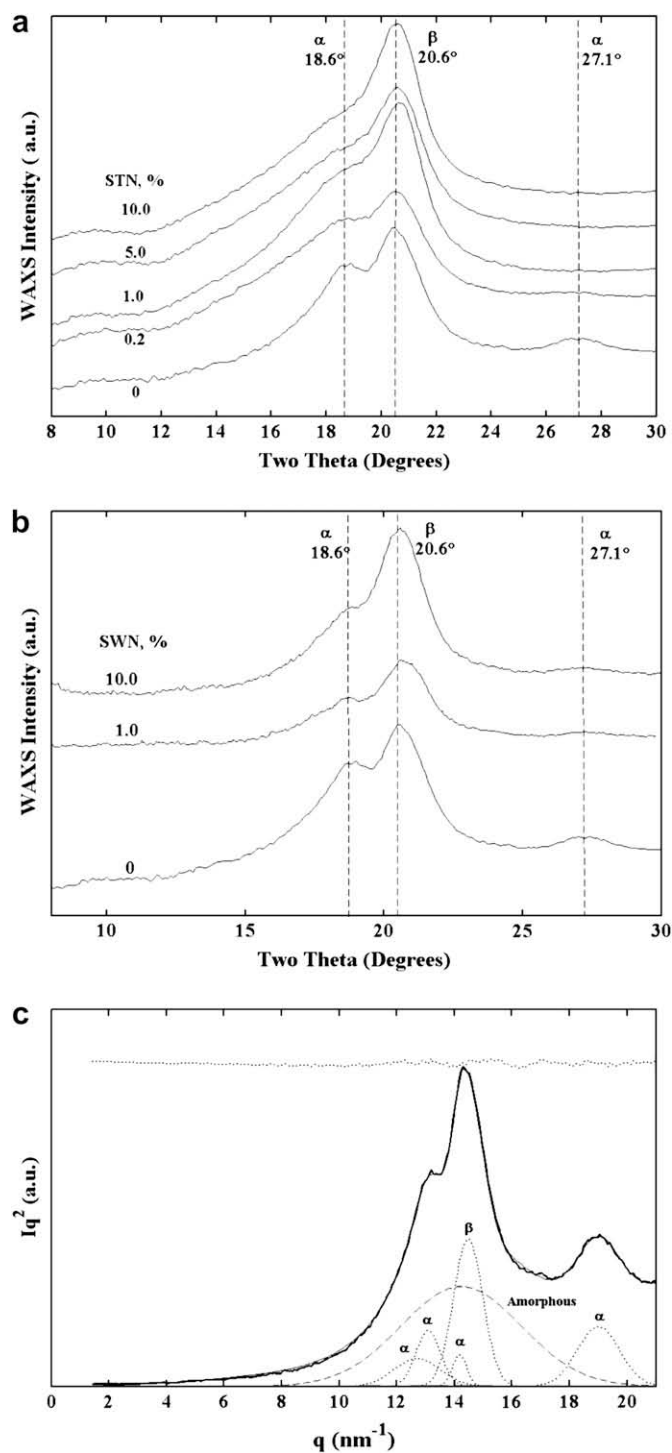


Fig. 3. Room temperature wide angle X-ray scattering intensity ($\lambda = 0.1542$ nm) vs. scattering angle, two theta, for electrospun composite nanofibers, at the nanoclay compositions indicated: (a) PVDF/STN; (b) PVDF/SWN. (c) Example of X-ray peak fitting for electrospun neat PVDF nanofiber. The heavy solid curve is actual data; the light solid curve is the fitted line. Above the curve is the residual (dotted line), the difference between the data and the fitted line. The individual fitted Gaussians are shown with dotted lines, for alpha and beta phase crystal reflections as marked. The amorphous halo is shown by a dashed line.

even 10% SWN do not have this remarkable ability to prevent alpha phase crystals from forming. In PVDF/SWN composite nanofibers we always observe the coexistence of alpha and beta phase crystals, even through the amount of alpha crystals does decrease as the

Table 1

Crystallinity index and ratio of alpha to beta crystals for ES PVDF and its nanocomposites.^a

Sample	ϕ_{ci}^b (± 0.01)	α/β^c (± 0.01)
Neat PVDF	0.46	1.30
SWN 1.0%	0.26	0.73
SWN 10.0%	0.33	0.65
STN 0.2%	0.35	1.29
STN 1.0%	0.20	0
STN 5.0%	0.22	0
STN 10.0%	0.26	0

^a Nanocomposites made with Lucentite™ STN or SWN nanoclays.

^b Mass fraction crystallinity calculated from WAXS ratio of crystal peak area to total peak area at room temperature.

^c Ratio of alpha crystal peak area to beta crystal peak area from WAXS at room temperature.

content of SWN increases. This demonstrates that hectorite itself has the effect of inhibiting the growth of non-polar alpha phase crystals, while promoting the growth of polar beta phase, but the ionic organic modifier in Lucentite™ STN greatly enhances this ability.

Fig. 4a–c shows the FTIR absorbance for all the electrospun PVDF composite nanofibers. PVDF/STN is presented in Fig. 4a. The bands at 614, 764, 796 and 976 cm^{-1} correspond to the TGTG' conformer of alpha phase PVDF, while the bands at 840 and 1274 cm^{-1} are considered to appear when the chain has a longer trans sequence than TT [31]. These bands are characteristic of β or γ phase crystals, which contain TTT or TTTGTTG', respectively. From the FTIR absorbance, we can see the alpha conformers disappear when 1% or more STN was added, confirming the results of X-ray analysis that the STN has the effect to impede the growth of the alpha phase.

The data in Fig. 4a can be normalized based on the absorbance peak at 877 cm^{-1} , which is regarded as proportional to the thickness of the sample and can be used as an internal standard [31]. We can see from the normalized FTIR absorbance in Fig. 4b that the electrospun PVDF homopolymer nanofibers have the smallest 1274 cm^{-1} and 840 cm^{-1} absorbance peak intensity. The 0.2% and 1% STN composite nanofibers show stronger peak intensities at these frequencies than pure PVDF. The electrospun PVDF/STN nanofibers containing 5% and 10% STN also have greater absorbance at 1274 cm^{-1} and 840 cm^{-1} than homopolymer PVDF. But 5% and 10% STN nanofibers absorb with almost the same peak value, which suggests that some agglomeration might have occurred in the nanoclay.

The bands at 811 and 1232 cm^{-1} , which are attributed to TTTG conformation in gamma phase [31,32], show a very slight increase with the increase of STN, which means the extended TTTG conformation is slightly enhanced by the addition of STN. Based on the literature [31], the 840 cm^{-1} peak is the indicator of trans chains longer than TT while 1274 cm^{-1} peak stands for much longer trans sequences, which are both attributed to beta phase. The tendency to form longer trans sequences in the electrospun composite nanofibers increases as more STN is added, which means the beta conformation is also increased by the STN. Crystallization favoring the extended PVDF polymorphs TTTT and TTTGTTG' in electrospun PVDF/nanoparticle nanofibers has previously been observed by Andrew et al. [25,33]. This result is also consistent with our recent work on electrospun PET nanofibers containing multi-walled carbon nanotubes (MWCNT) as the inclusion [30]. In that work, trans sequences increased due to chain confinement, even for low degrees of crystallinity of the PET/MWCNT nanofibers.

Fig. 4c shows FTIR absorbance for PVDF/SWN composite nanofibers. From the FTIR absorbance we can see the alpha phase bands at 614, 763 and 796 cm^{-1} do not show a regularly decreasing trend with composition. However, the intensity of characteristic beta and

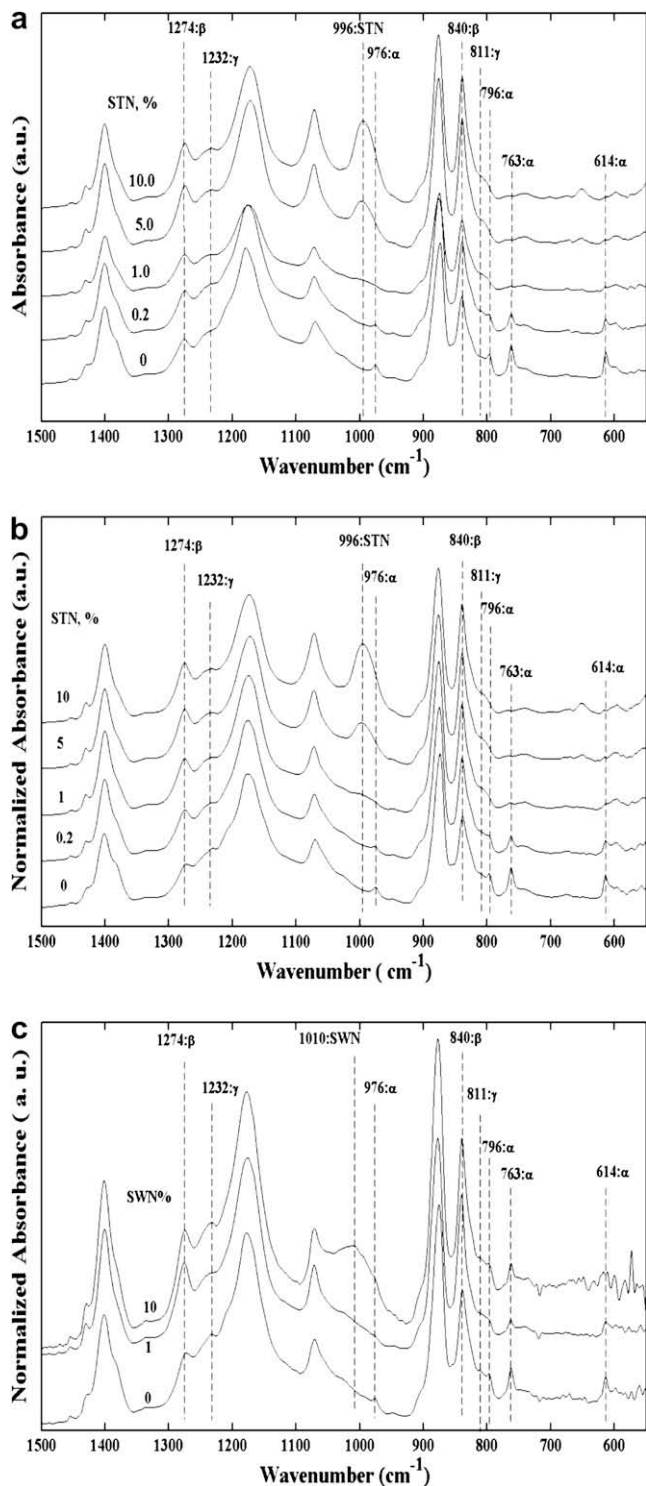


Fig. 4. (a) FTIR absorbance vs. wavenumber for electrospun PVDF/STN composite nanofibers; (b) Normalized FTIR absorbance vs. wavenumber for electrospun PVDF/STN composite nanofibers; (c) Normalized FTIR absorbance vs. wavenumber for PVDF/SWN composite nanofibers. Curves are shifted vertically for clarity in all parts of the figure.

gamma bands still has observable increase with increasing amount of SWN. X-ray results in Fig. 3b confirm that the alpha crystal phase cannot be totally eliminated by the addition of SWN. Both X-ray and FTIR results demonstrate that SWN does not have the same ability as STN to impede the formation of the alpha phase while enhancing the beta and gamma phases in electrospun PVDF/Nanoclay composite nanofibers.

We suggest a mechanism to explain why the addition of STN nanoclay has the effect of increasing the extended TTT conformations while impeding TG conformations. Based on the paper by Yee, et al. [24] the addition of 3 wt% tetrabutylammonium chloride (TBAC) can increase the beta phase in electrospun PVDF fibers. They explain their results by suggesting that TBAC can retain water molecules which will form hydrogen bonds with the fluorine atoms in PVDF, inducing the beta crystal phase to form. The organic modifier in the STN nanoclay has a very similar structure to the TBAC salt. Yee, et al. [24] examined the O–H stretching vibration at 3400 cm⁻¹ and declared that this proved the existence of hydrogen bonds in PVDF/TBAC fibers. However, from our FTIR results, there was no peak at all in the vicinity of 3400 cm⁻¹ (data not shown in the interests of brevity). Thus, in the electrospun PVDF/STN composite nanofibers no O–H or N–H bonds appear to be formed upon the addition of the STN nanoclay to PVDF.

In Fig. 5 the FTIR absorbance, normalized to the band at 877 cm⁻¹, shows the electrospun PVDF/STN composite nanofiber in the higher wavenumber range. The 2853 cm⁻¹ and 2926 cm⁻¹ bands stand for the symmetric and asymmetric CH₂ stretching vibrations, respectively [34–36]. These two peaks decrease systematically when STN nanoclay is added to PVDF, which means the STN has the effect of impeding the motion of the CH₂ molecular stretch. The CH₂ stretch may arise from either the PVDF monomer, or from the alkane group from the organic modifier of the nanoclay. Although the total amount of CH₂ increased after we added more nanoclay, the normalized absorbance peak intensity for the CH₂ stretching vibrations still decreased, which means the CH₂ vibrations were blocked, probably due to strong interaction with the surrounding groups.

It has been recognized for more than two decades that PVDF would crystallize preferentially into the beta phase when films were cast from certain solvents, such as DMF [39]. More recently, Salimi and Yousefi [38] proposed that the polymer–solvent interaction might be the reason for the increased beta phase observed in PVDF/DMF solutions evaporated at 50 °C. In the case of addition of nanoclay, the interaction may be between the ions of the nanoclay and the dipole moment of the PVDF chain. The nanoclays have negative charges distributed on their platelets (see Scheme 1) because of the isomorphous substitution within the layers (Al³⁺ replaced by Mg²⁺ or Mg²⁺ replaced by Li⁺) [2,37] to balance the positive cations contained in between. The STN and SWN nanoclays might both have a similar ability to bond with the PVDF chain because of the negative charge on the layered silicate hectorite,

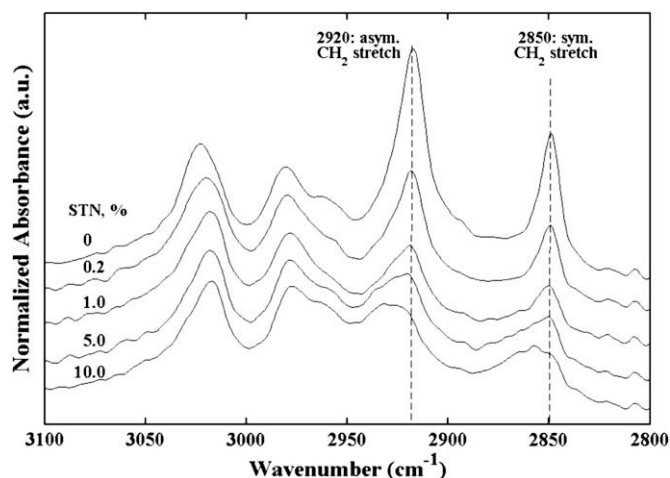


Fig. 5. FTIR absorbance vs. wavelength showing the CH₂ stretching vibration region for all concentrations of PVDF/STN electrospun composite nanofibers.

$\text{Na}_{0.33}(\text{Mg}_{2.67}\text{Li}_{0.33})(\text{Si}_4\text{O}_{10})(\text{OH})_2$ in SWN and STN. As suggested by Ramasundaram et al. [23] the partially positive CH_2 dipoles on the PVDF chains could have an ion–dipole interaction with the negatively charged nanoclay platelets and make the polymer chains align on the surface of hectorite, which will enhance the extended TTT conformers and result in formation of the beta crystallographic phase. The tiny amount of TTTGTTG' conformers existing in the nanofiber is likely due to the gauche effects formed from local internal chain rotation as suggested by Ramasundaram et al. In the case of electrospun nanofibers, the rotation stems from the static electric force during the process of electrospinning instead of high temperature in the melt crystallization process. In the case of electrospun nanofibers, Fig. 6 shows the possible interaction mechanism between the nanoclay and PVDF chains [40,41].

For comparison, we evaporated PVDF solution (the same as that which was used for electrospinning) at around 50°C , and obtained raw film. FTIR absorbance of PVDF film and electrospun fiber is shown in Fig. 7. The PVDF raw film displays only the 840 cm^{-1} beta peak, and 811 cm^{-1} and 1232 cm^{-1} gamma peaks, which means there are some TTT and TTTG conformations present in the film but no long trans chains or TGTG' conformers. In contrast, the PVDF electrospun fiber has very strong alpha peaks at 614 , 763 and 976 cm^{-1} , which means the electrospinning process can induce more TG conformations in PVDF. The PVDF polymer chain is highly polar, with dipole moment of the TGTG' repeat equal to $3.4 \times 10^{-30}\text{ Cm}$ along the chain direction and $4.0 \times 10^{-30}\text{ Cm}$ normal to the chain. For beta phase conformer of the type TTTT, the dipole moment per repeat is $7.0 \times 10^{-30}\text{ Cm}$ essentially normal to the chain. Thus, the PVDF dipole moment can more easily align in the applied external electric field during the electrospinning process. PVDF crystallizes in the process of electrospinning in the presence of the static electric force. The co-electrospinning with STN nanoclay could decrease the formation of gauche conformations because STN has the ability to bond with the PVDF monomer by ion–dipole interaction. As shown in the model picture of Fig. 6, the nanoclay aligns the CH_2 dipole to one side, inducing more beta phase to crystallize during electrospinning, as proposed by Ramasundaram et al. [23].

3.3. Thermal properties

Finally, we show thermal analysis of the electrospun PVDF nanocomposites. DSC heat flow vs. temperature is shown in Fig. 8 for electrospun PVDF/STN composite nanofiber samples. PVDF and

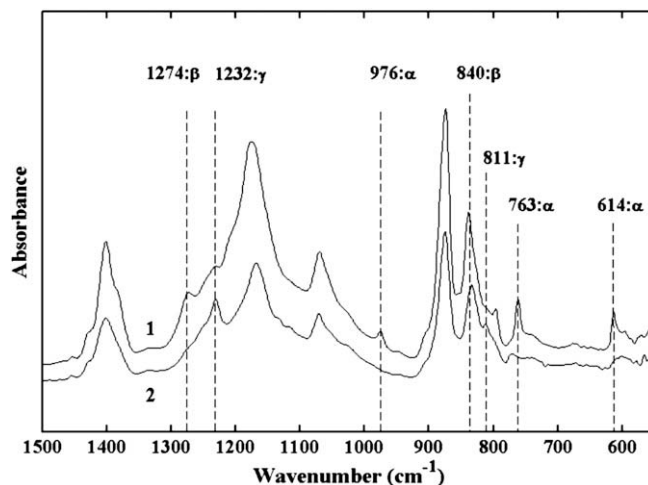


Fig. 7. FTIR absorbance vs. wavenumber of PVDF electrospun fiber (curve 1) and PVDF evaporated film (curve 2).

PVDF/STN 0.2% only have one major melting endotherm at 164.2°C , which can be described as a superposition of the melting peaks for the alpha and beta phase crystal. In PVDF with 1.0%, 5.0% and 10% STN, there are two or three endotherms observed at around 164°C , 169°C , and 174°C which are partly overlapped and superimposed. The lowest endotherm most likely results from recrystallization in the process of heating. The middle and the upper melting endotherms may result from the final melting of beta phase crystals that reorganized during the heating. The glass transition region occurs at lower temperature and is not shown in the interests of brevity; T_g did not change much with nanoclay addition. Thermal properties are listed in Table 2 including T_g and crystallinity calculated from the area of the endotherm. The electrospun PVDF/STN composite nanofibers have smaller crystallinity than neat PVDF nanofiber, which is consistent with results from X-ray. However, the results for absolute crystallinity are not comparable between X-ray and DSC. The ES fibers are crystallizing under the conditions of rapid solvent removal. WAXS data are taken at room temperature, whereas the DSC scans reflect the state of the crystals after perfection during heating.

Thermal stability and molecular retraction were assessed for several ES fiber mats. During electrospinning, the molecular chains of PVDF become aligned to a state of low entropy along the

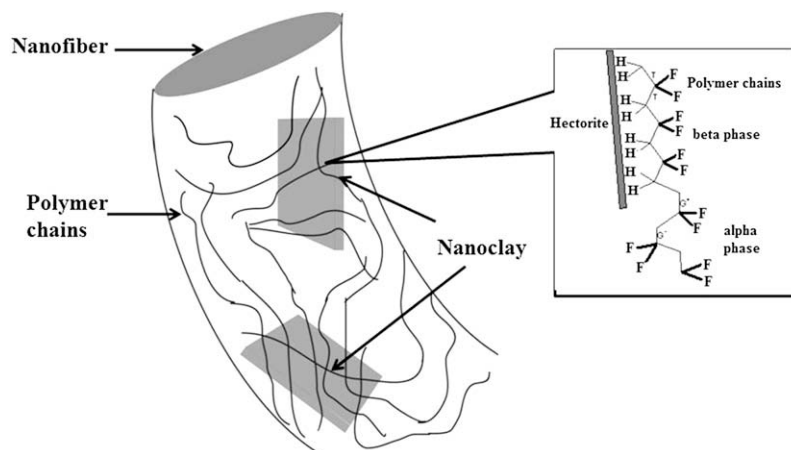


Fig. 6. The possible interaction between hectorite and PVDF chain in the electrospun composite nanofiber: partially positive C–H bond is attracted by the negatively charged silicate layer in STN and SWN due to the static electric force.

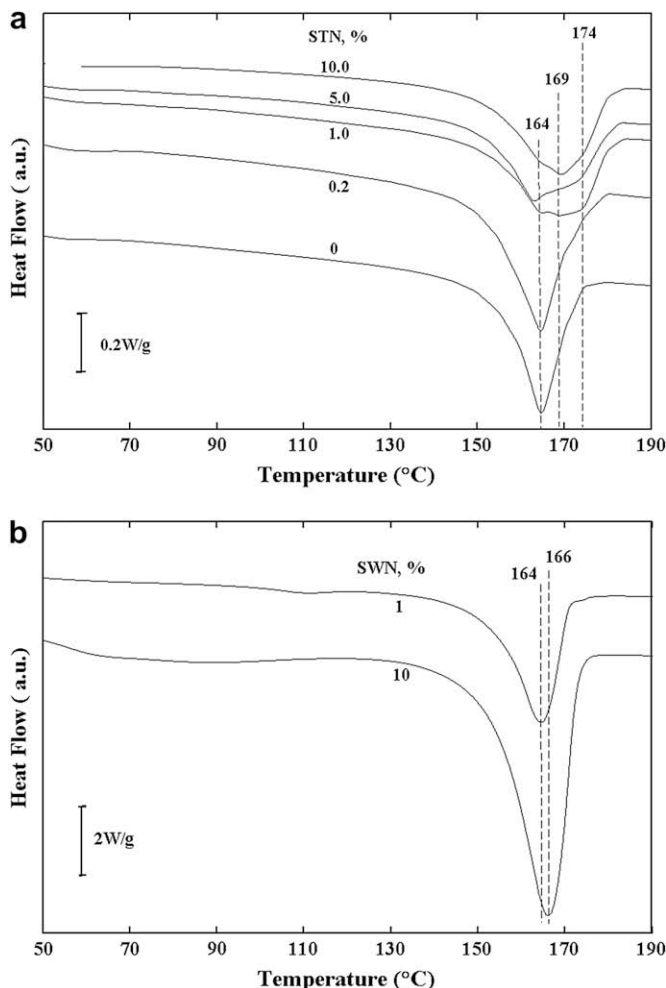


Fig. 8. DSC heat flow vs. temperature for all electrospun nanofibers, at 10 °C/min. (a) PVDF/STN (b) PVDF/SWN composite nanofibers.

fiber axis. When the membranes are heated, the surface area retracts to a random coil state of higher entropy. To observe this mechanism, membranes of pure PVDF and composite nanofibers with STN and SWN were placed directly into oil and heated to around 170 °C, which is slightly higher than the melting peak temperature of the PVDF crystals. Before the melting point, there is no observable retraction for the membranes, because the crystals act as thermoreversible crosslinks. Once the crystals start to melt, the surface area of the nanofiber membrane began to shrink due to molecular retraction of the elongated polymer chains.

If A_0 is the initial surface area of a given membrane, and under the assumption that the thickness of the membrane does not change, we may characterize the retraction by comparing A_0 to the final surface area after crystal melting, A_f . The area retraction for pure PVDF is $A_f = 0.42A_0$; for nanofiber composites with 1.0% STN, $A_f = 0.044A_0$, and for nanofiber composites with 1.0% SWN, $A_f = 0.070A_0$. Thus a 1.0% addition of nanoclay results in substantial retraction of the surface area compared to the homopolymer ES nanofiber mat. However, when the nanoclay content in the nanofiber composite increased to 10%, the area shrinkage was less (i.e., final surface area was greater) than in the 1% nanofiber composites: for STN10%, $A_f = 0.095A_0$, and for SWN10%, $A_f = 0.310A_0$.

The addition of nanoclay increases the elongation in the co-electrospun nanofibers and therefore makes the composite nanofibers

Table 2

Thermal properties^a for ES PVDF and its nanocomposites with STN and SWN nanoclay.

Sample	T_g (°C) ^b (± 0.2)	χ_c ^c (± 0.01)
Neat PVDF	-29.2	0.47
SWN 1.0%	-27.8	0.47
SWN 10.0%	-29.1	0.42
STN 0.2%	-29.0	0.45
STN 1.0%	-28.8	0.43
STN 5.0%	-29.8	0.47
STN 10.0%	-28.1	0.44

^a Data taken during DSC scanning at 10 °C/min.

^b Glass transition temperature determined from the inflection point of the heat capacity step.

^c Degree of crystallinity calculated from DSC endotherm area using 104.6 J/g for heat of fusion of 100% crystalline PVDF [26].

retract more than the neat ES polymer. As the polymer nanofiber is co-electrospun with nanoclay, the polymer chains will be attracted to the clay platelets and elongated by the electric force during the electrospinning process. Then, the crystals that form in the ES nanofiber mats serve as thermoreversible crosslinks to prevent the polymer chains from retracting. When the nanofibers are heated to the crystal melting point, these physical crosslinks are removed and the polymer chains will gain the mobility so that they are able to shrink due to the elastic force from elongation.

The retraction of STN is slightly larger than the SWN and the difference becomes more obvious at higher clay concentration. The STN is better dispersed and interacts with the polymer chains causing more elongated polymer chains in the STN nanofibers resulting in a larger retraction once they are heated. The lower area retraction in 10% compared to 1.0% loading of nanoclay indicates the overdosed nanoclay will have negative effect to the formation of aligned polymer chains in ES nanofibers. From this experiment, we also noticed that the nanofiber composite membrane containing SWN started to retract at a lower temperature and qualitatively retracted faster than the nanofiber composite membrane containing STN. SWN nanoclay does not contain any organic modifier, so it has much weaker interaction with the polymer chains than does the organically modified STN nanoclay. This may cause the elongated polymer chains in the nanofiber composites with SWN to retract more easily than the ones with STN, which has stronger interaction with polymer chains and therefore increases the energy for the retraction to occur. More detailed experiments about molecular retraction in ES nanofiber composites are underway, and will be presented in a future work.

4. Conclusions

We investigated the morphology and crystal polymorphism of electrospun PVDF/Nanoclay composite nanofibers for the first time. In our study, we used two kinds of synthetic layered silicate nanoclays: organically modified STN and plain hectorite SWN. Based on our result we conclude the following:

1. The addition of STN increases the uniformity of the diameter of the electrospun nanofiber while decreasing the number of beads inside the composite nanofibers. The reason is that the nanoclay contributes more ionic charges into the electrospinning solution, and therefore increases the conductivity of the system, which is known to make the electrospun nanofibers more uniform.
2. The molecular retraction experiment shows that the addition of nanoclay make the ES nanofibers retract more

than pure ES polymer nanofiber. The organically modified STN is more effective than unmodified SWN in bonding with the polymer chains so that more aligned polymer chains could be formed in the process of co-electrospinning, making the nanofiber composite retract more than neat PVDF nanofiber. Stronger interaction between STN and the polymer chains makes the nanofibers containing STN retract more than those containing unmodified SWN nanoclay.

3. WAXS result shows that both SWN and STN can enhance the beta crystallographic phase while impeding the growth of alpha phase. Due to the attachment of the ionic organic modifier, STN is much more effective than SWN in forming beta phase crystals. The FTIR results also demonstrate that without ionic modifier, SWN is much less effective in reducing the short-range alpha phase conformers. The nanoclay platelets are negatively charged due to the isomorphous substitution, which counterbalances the charge of the positive cations contained between the silicate layers. On the other hand, according to Ramasundaram et al. [23], the C–H bonds in PVDF monomer are partially positively charged, which results in ion–dipole interaction with the negatively charged nanoclay platelets. This interaction will align the PVDF polymer chains to form more TTTT and TTTGTTTG conformers and consequently, more beta and gamma phase crystals. The SWN without any organic modifier is much less effectively dispersed in the nanofibers, and results in fewer trans conformers reducing the amount of beta crystals in the ES composite nanofibers.

Acknowledgement

The authors thank the Petroleum Research Fund of the American Chemical Society, 44149-AC7; the National Science Foundation Polymers Program of the Division of Materials Research, DMR-0602473; and a Tufts University Faculty Research Award for financial support of this research. We thank the National Science Foundation MRI Program under DMR-0520655 for thermal analysis instrumentation. The SEM work was carried out at the Harvard University Center for Nanoscale Systems.

References

- [1] Alexandre M, Dubois P. *Mater Sci Eng R* 2000;28:1.
- [2] Ray SS, Okamoto M. *Prog Polym Sci* 2003;28:1539.
- [3] Huang ZM, Zhang YZ, Kotaki M, Ramakrishna S. *Compos Sci Technol* 2003; 63:2223.
- [4] Qin XH, Wang SY. *J Appl Polym Sci* 2006;102:1285.
- [5] Choi SW, Kim JR, Ahn YR, Jo SM, Cairns EJ. *Chem Mater* 2007;19:104.
- [6] Choi SS, Lee YS, Joo CW, Lee SG, Park JK, Han KS. *Electrochim Acta* 2004; 16:1151.
- [7] Gao K, Hu XG, Dai CS, Yi TF. *Mater Sci Eng B* 2006;131:100.
- [8] Gopal R, Kaur S, Ma ZW, Chan C, Ramakrishna S, Matsuura T. *J Membr Sci* 2006;281:581.
- [9] Lovinger AJ. *Science* 1983;220:1115.
- [10] Humphrey JS, Amin-Sanayei R, editors. *Vinylidene fluoride polymers*. New York: Wiley; 2002.
- [11] Davies GR. *Physics of dielectric solids*. In: Goodman C, editor. *Inst phys conf Series No.58*; 1980.
- [12] Humphreys J, Ward IM. *J Appl Polym Sci* 1985;30:4069.
- [13] Humphreys J, Lewis ELV, Ward IM. *J Polym Sci Part B Polym Phys* 1988;26:141.
- [14] Sajakiewicz P, Wasiak A, Gocłowski Z. *Eur Polym J* 1998;18:1945.
- [15] Southgate PD. *Appl Phys Lett* 1976;28:250.
- [16] Bamji SS, Kao KJ, Perlman MM. *J Polym Sci* 1980;18:1945.
- [17] McKinney JE, Davis GT, Broadhurst MG. *J Appl Phys* 1980;51:1676.
- [18] Priya L, Jog JP. *J Polym Sci Part B Polym Phys* 2002;40:1682.
- [19] Dillon D, Tenneti K, Li C, Ko F, Sics I, Hsiao B. *Polymer* 2006;47:1678.
- [20] Buckley J, Cebe P, Cherdack D, Crawford J, Ince BS, Jenkins M, et al. *Polymer* 2006;47:2411.
- [21] Prest W, Luca D. *J Appl Phys* 1975;46:4136.
- [22] Prest W, Luca D. *J Appl Phys* 1978;49(10):5042.
- [23] Ramasundaram S, Yoon S, Kim KJ, Park C. *J Polym Sci Part B Polym Phys* 2008;46:2173.
- [24] Yee WA, Kotaki M, Liu Y, Lu X. *Polymer* 2007;48:512.
- [25] Andrew JS, Mack JJ, Clarke DR. *J Material Res* 2008;23:105.
- [26] Nakagawa K, Ishida Y. *J Polym Sci Polym Phys* 1973;11:2153.
- [27] Li D, Xia Y. *Adv Mater* 2004;16:1151.
- [28] Bachmann M, Lando J. *Macromolecules* 1981;14:40.
- [29] Hasegawa R, Takahashi Y, Chatani Y, Tadokoro H. *Polym J* 1972;3:600.
- [30] Chen H, Liu Z, Cebe P. *Polymer* 2009;50:872.
- [31] Tashiro K, Kobayashi M, Tadokoro H. *Macromolecules* 1981;14:1757.
- [32] Bachmann M, Gordon W, Koenig J, Lando J. *J Appl Phys* 1979;50:6106.
- [33] Andrew JS, Clarke DR. *Langmuir* 2008;24:8435.
- [34] Arimoto H. *J Polym Sci Part A* 1964;2:2283.
- [35] Skrovanek DJ, Howes SE, Painter PC, Coleman MM. *Macromolecules* 1985;18:1676.
- [36] Schroeder LR, Cooper SL. *J Appl Phys* 1976;47:4310.
- [37] Paul DR, Robeson LM. *Polymer* 2008;49:3187.
- [38] Salimi A, Yousefi A. *J Polym Sci Part B Polym Phys*. 2004;42:3487.
- [39] Lovinger AJ. *Poly(vinylidene fluoride)*. In: Bassett DC, editor. *Developments in crystalline polymers: polymers-1*. London: Applied Science Publisher Ltd.; 1982. p. 215–6.
- [40] Fong H, Liu WD, Wang CS, Vaia RA. *Polymer* 2002;43:775.
- [41] Li L, Bellan LM, Craighead HG, Frey MW. *Polymer* 2006;47:6208.